A Round Earth Loss Model and Small-scale Channel Properties for Open-Sea Radio Propagation

Kun Yang, *Member, IEEE*, Andreas F. Molisch[†], *Fellow, IEEE*, Torbjörn Ekman, *Member, IEEE*, Terje Røste, *Life Member, IEEE*, and Marion Berbineau, *Member, IEEE*

***Abstract*—In this paper, a path-loss model for the open-sea environment is proposed, in which different propagation phenomena including effective reflection, shadowing, divergence, and diffraction, related to the sea surface and earth curvature in the open-sea environments, are taken into account. The channel model is parameterized and validated by experimental results from our measurement campaign at 2 GHz over a distance range of 45 km in calm, cold Norwegian ocean waters. Model and measurements show excellent agreement in terms of the Root Mean Square Error (RMSE). By evaluating the channel model parameters like mean-square surface slope and standard deviation of surface height related to the sea surface roughness, it can be concluded that the effects of shadowing and scattering on the reflected rays will influence the fading amplitude within the distance range where the LOS is tangential to the surface of the earth. It is also found that the diffraction loss starts to influence the path-loss results beyond the distance of 0.6 times the First Fresnel Zone clearance. The amplitude probability density function (PDF) of fading is studied as well. By using the Akaike information criterion (AIC) for model selection, it is found that the amplitude PDF can be modeled as Weibull distribution at short distances and very large distances. The TWDP distribution, Rician distribution and Rayleigh distribution dominate at distances between 9 km and 45 km. The correlation coefficient between the signal amplitudes at two antennas that are vertically separated by 3 m was studied, and found to be close to zero when the TX is below the horizon. This indicates the potential to employ multi-antenna techniques for maritime communication systems.**

I. Introduction

Reliable and high throughput maritime communications are considered to play an important role in maritime activities involving various types of ships and vessels, offshore installations, unattended buoy platforms, autonomous underwater utilities, offshore and onshore observation sites, etc. Most of these activities occur within the exclusive economic zone (EEZ) of a country, defined as an area extending to a distance of 200 nautical miles (370.4 km) from its costal baseline. However, many of these communication activities will happen over somewhat shorter distances; e.g. the distance limit for the offshore broadband service in Norway will be 70 km from the coastline, which was regulated by the Norwegian Communication Authority in 2018 [1].

Current maritime communication systems like satellite systems and VHF suffer from the disadvantages of high cost and low data rates, respectively. Cellular communication systems like 4G LTE, WiFi and WiMAX, originally designed for terrestrial propagation environments, can not perform optimally in maritime propagation environments [2], [3]. Designing improved communication systems, e.g, by optimizing current WiFi and LTE systems and designing dedicated 5G maritime solutions, requires first of all an understanding of the maritime radio propagation channel, in particular path loss and fading.

In previous studies, the Plane Earth Loss (PEL) model [4], was widely used to compare with the measured path-loss results obtained from maritime propagation environments [2], [5], [6], [7]. However, the PEL assumption of a plane earth surface inherent in this model is not fulfilled for maritime radio links at larger distances, as has been pointed out in [7], [8]. This is due to the fact that the diffraction loss caused by the earth curvature and sea roughness can not be ignored. A method for point-to-area predictions of field strength for the maritime mobile services in the frequency range of 30 MHz to 3000 MHz, and for distances in the range 1 km to 1000 km, was proposed in the ITU-R Recommendation P.1546-5 [9]. However, the evident deep fades at short TX-RX distances found in multiple previous measurement campaigns [2], [5], [6], [7], [10] are not taken into account, which has been pointed out in [11], [12], [13]. As a first step to remedy this situation, we proposed in [8] a quasi-deterministic path-loss model integrating the PEL model at short TX-RX distances with the ITU-R model at large TX-RX distances by using a proper blending method. However, several propagation phenomena still have not been taken into consideration. These are the joint effects of scattering and shadowing due to the rough sea surface, and divergence and diffraction due to earth curvature. In addition, the amplitude probability density function (PDF), which is essential for communication system design, has not been investigated for the 2 GHz frequency band

Manuscript received June 19, 2018; revised November 7, 2018 and May 5, 2019; accepted June 25, 2019. The work of K. Yang, T. Ekman, and T. Røste was supported by the MAMIME project under Grant 256309 by Norwegian Research Council. The work of A. F. Molisch was supported by National Science Foundation. The review of this paper was coordinated by Prof. F. Paris. This paper was presented in part at the IEEE VTC 2011, Budapest, Hungary, May 2011 and in part at the IEEE VTC 2013, Las Vegas, NV, USA, September 2013.(*Corresponding author: Kun Yang.*)

K. Yang and T. Røste are with the Super Radio AS, 0556, Oslo, Norway (e-mails: kun@superradio.no; terje@str.no).

A. F. Molisch is with the Department of Electrical and Computer Engineering, Viterbi School of Engineering, University of Southern California, Los Angeles, California, 90089, USA (e-mail: molisch@usc.edu).

T. Ekman is with the Department of Electronics and Telecommunications, Norwegian University of Science and Technology (NTNU), 7491 Trondheim, Norway (e-mail: torbjorn.ekman@iet.ntnu.no).

M. Berbineau is with the Univ. Lille Nord de France, IFSTTAR, COSYS, LEOST, F-59650 Villeneuve d'scq, France (e-mail: marion.berbineau@ifsttar.fr).

Digital Object Identifier 10.1109/TVT.2019.2929914

with ranges up to 45 km. The current paper aims to address these aspects, and provides a comprehensive and accurate channel model for TX-RX distances up to 45 km within the EEZ, parameterized by measurements in cold, calm sea. In particular, this paper makes the following contributions:

1) Proposing a theoretical model that takes into account scattering by the rough sea surface, beam divergence, and shadowing.
2) Presentation of results from an extensive measurement campaign in Norway in cold, calm sea, and comparison of path-loss measurements to the theoretical model.
3) Investigation of the small-scale fading distribution as a function of the distance between TX and RX.
4) Study of the spatial correlation coefficient between vertically separated antennas on shore.

The rest of the paper is organized as follows: In section II the measurement campaign is described briefly. Section III discusses our round earth loss model in detail. Section IV is devoted to the estimation and parameterization of the small-scale fading. Finally, conclusions are drawn in section V.

II. Measurement Campaign

The measurements were performed with a wideband channel sounder operating at 2.075 GHz carrier frequency. The sounding signal was a chirp waveform with a bandwidth of 20 MHz. Different chirp intervals (corresponding to different Doppler frequency resolutions) were used during the measurements. A detailed description of the channel sounder is given in [10], [11].

The receiver (RX) was in a van connected to two antennas close to the shore. Two vertically polarized sector antennas possessing 15 dBi gain and $30°$ 3 dB beamwidth were mounted with a vertical spacing of 2.9 m (see Fig. 1(a)). The "nominal" height of the lower antenna above sea level was 11.2 m without taking the tidal wave changes into consideration. At the transmitter (TX) side, the same type of sector antenna was installed on the ship, with an antenna height of 9.5 m above the sea level (see Fig. 1(b)). The ship was equipped with an Automatic Identification System (AIS), from which the recorded GPS data and ship speed can be obtained. The TX antenna pointing was adjusted to face the RX antenna accordingly when the ship changed its direction from the outbound trip (away from the RX) to the inbound trip (towards the RX, see Fig 2), so that the main beam always pointed towards the RX. Since the superstructure of the boat caused reflections during the inbound trip, only the received signal level (RSL) results from the outbound trip are used to validate the Round Earth Loss (REL) model in this paper. The total measured distance range covers about 45 km and the ship route in the Trondheimfjorden is shown in Fig. 2. During the whole measurement, the weather was calm and cold, which can be categorized as Douglas Sea State 3. It is important to note that the parameterization and experimental validation of the model is thus also restricted to this type of sea state. The ship was travelling at a constant speed of 6 knots $\approx 3.1\ \mathrm{m/s}$). The main parameters of the measurement setup and environments can be found in Tab. I. More details about the measurement setup and the campaign can be found in [10].

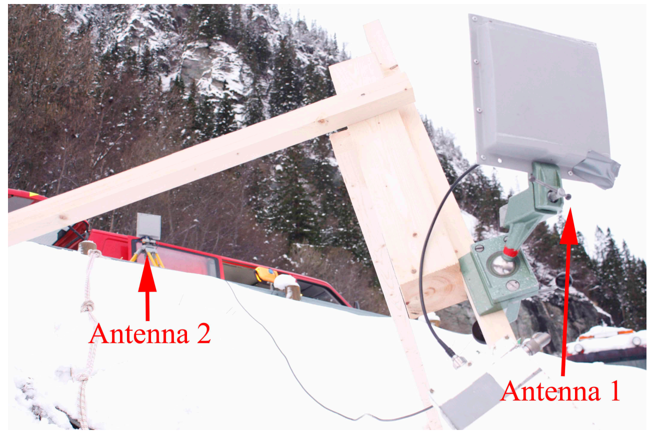

(a) Receiver (RX) antennas on the shore.

(b) Transmitter (TX) antenna at the ship.

Fig. 1. Receiver and transmitter antennas of the channel sounder

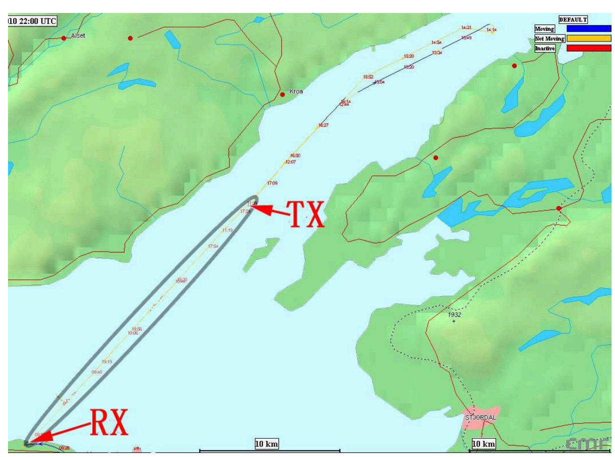

Fig. 2. The route of the ship.

TABLE I
THE MEASUREMENT PARAMETERS

Carrier frequency	2.075 GHz
Chirp bandwidth	20 MHz
Transmitting power at the antenna port	27.2 dBm
Maximum delay span	40.96 μs
Delay resolution	50 ns
Doppler resolution	4, 0.5, 0.25, 0.125, 0.0625 Hz
Maximum Doppler shift span	±128 Hz
Number of TX antennas	1
Number of RX antennas	2
TX and RX antenna gain	15 dBi
3 dB Antennas beamwidths	$30°(Az.) \times 30°(El.) Approx$
RX sensitivity	-110 dBm
TX antenna height	9.5 m
Lower RX antenna height	11.2 m
Vertical spacing between RX antennas	2.9 m
Maximum route distance	45 km
Temperature	[-1, 2] °C
Wind speed	[3, 6] m/s
Boat speed	6 knots $\approx 3.1\ m/s$

III. A Round Earth Loss Model

As mentioned in Section I, the evident deep fades at short TX-RX distances are found in several maritime measurement results at different frequency bands (up to 17 dB at 2 GHz in Norwegian cold sea under the weather conditions of Douglas Sea State 3 [10] and up to 10 dB at 5.2 GHz in the Baltic sea [13]). These propagation 'holes' can dramatically influence the system performance, which has been proved by the UDP and TCP throughput results of the WiFi test in Portugal under the weather conditions of Douglas Sea State 3 and 10 degree Celsius [3]. These propagation holes can cause negative effects on the navigation and security system, which makes it important to have path-loss models that can provide accurate predictions. The classical PEL model can predict these holes if TX-RX distances are within the breakpoint distance [7], [8], where the first Fresnel zone touches the ground. This indicates a geometrical dependence between the path-loss results and the antenna heights. However, the PEL model is not valid at large distances, i.e., beyond the radio horizon. Therefore, a more comprehensive geometrical model is given in this section by taking the earth curvature into consideration. The amplitude of the deep fades are also found to be smaller than the results predicted by the PEL model with idealized specular reflections [8], which means that the effective reflection coefficient, accounting for the roughness of the surface, and the shadowing effect for the reflected ray need to be taken into account. In addition, the increasing offset between the measured RSL and the RSL predicted by the PEL model shows the importance of the effective reflection coefficient from the rough sea surface and the diffraction loss due to gradual shadowing by the earth curvature when the TX-RX distances increase. The round earth loss model [14] is obtained by using a spherical geometry and the diffraction, shadowing and reflection corrections for a two-ray model. The following effects based on the two-ray model need to be accounted for:

$$\begin{cases} \text{LOS} \begin{cases} \text{Free space Loss} \\ \text{Diffraction Loss} \end{cases} \\ \\ \text{Sea Reflection} \begin{cases} \text{Effective Reflection} \\ \text{Divergence} \\ \text{Shadowing Effect} \\ \text{Diffraction Loss} \end{cases} \end{cases} \quad (1)$$

A. Geometrical model

Since the earth can not be considered to be 'plane' for our distances of interest, a round earth geometrical model based on the two-ray method is proposed, which is shown in Fig. 3. The earth radius ($\sim$ 6371 km) is denoted by r_e and d is defined as the projection of the TX-RX distance onto the earth surface shown in Fig. 3. Parameter h_1 and h_2 denote the TX and RX antenna height, respectively. P_TX and P_RX are transmitted and received powers at the terminal of the respective antennas. According to the geometric relations shown in Fig 3, P_RX is obtained as:

$$\frac{P_\mathrm{RX}}{P_\mathrm{TX}} = \left(\frac{\lambda}{4\pi D_\mathrm{LOS}}\right)^2 \left|1 + R \cdot exp(jkD_\mathrm{diff})\right|^2 \quad (2)$$

where R and D_LOS are the reflection coefficient from the sea surface and the path length of the LOS, respectively. D_diff represents the path length difference between the LOS and sea reflection expressed in (2). It needs to be mentioned that an unambiguous solution can be obtained by choosing the smallest values of alpha and beta that satisfy (9) and (10).

$$D_\mathrm{diff} = X_1 + X_2 - D_\mathrm{LOS} \quad (3)$$

$$d = D_1 + D_2 \quad (4)$$

where

$$D_\mathrm{LOS} = \sqrt{(r_\mathrm{e} + h_1)^2 + (r_\mathrm{e} + h_2)^2 - \xi} \quad (5)$$

$$\xi = 2(r_\mathrm{e} + h_1)(r_\mathrm{e} + h_2)\cos\left(\frac{d}{r_\mathrm{e}}\right) \quad (6)$$

The distances X_1 and X_2 can be obtained as

$${X_1}^2 = (h_1 + r_\mathrm{e})^2 + {r_\mathrm{e}}^2 - 2(r_\mathrm{e} + h_1)r_\mathrm{e}\cos\alpha \quad (7)$$

$${X_2}^2 = (h_2 + r_\mathrm{e})^2 + {r_\mathrm{e}}^2 - 2(r_\mathrm{e} + h_2)r_\mathrm{e}\cos\beta \quad (8)$$

and α and β can be obtained from:

$$\arccos\left(\frac{r_\mathrm{e} + h_1 - r_e cos\alpha}{X_1}\right) + \alpha = ... \\ \arccos\left(\frac{r_\mathrm{e} + h_2 - r_e cos\beta}{X_2}\right) + \beta \quad (9)$$

$$\alpha + \beta = \frac{d}{r_\mathrm{e}} \quad (10)$$

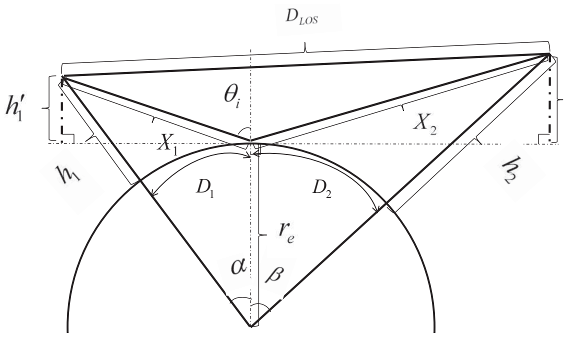

Fig. 3. Geometrical model for the REL model.

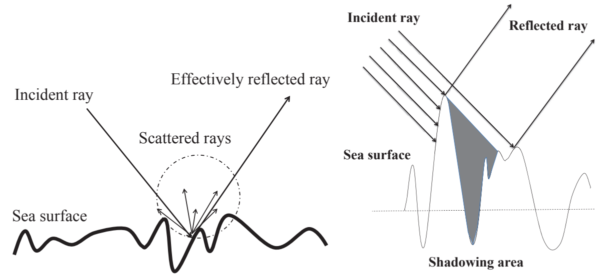

(a) Effective reflection. (b) Shadowing effect.

Fig. 4. Effective reflection and Shadowing effect by a rough sea surface

B. Propagation phenomena

1) Effective reflection from a rough sea surface: The roughness of sea surface due to sea movement makes the specular reflection model unsuitable for mobile radio signals, especially when big-wave surfaces are occurring during bad weather conditions. Since part of the reflected power will be scattered into other directions as shown in Fig. 4(a), a power reduction of the specular reflected ray needs to be taken into consideration. The height variations of rough sea surface can be modeled as Gaussian-distributed [15], [16], [17]. We furthermore assume for the moment that no shadowing effect occurs on the rough surface (i.e., no wave crest is shadowing off a trough); this assumption will be relaxed below. Under these two conditions, the Kirchhoff theory [15] of scattering is valid, and the effective reflection coefficient R_{rough} can be expressed as:

$$R_{\mathrm{rough}} = R \cdot \exp[-2\left(\frac{2\pi\sigma_{\mathrm{h}} sin\theta_{\mathrm{e}}}{\lambda}\right)^2] \tag{11}$$

where

$$\begin{aligned} h'_1 &= h_1 - 0.5 r_{\mathrm{e}}\alpha^2 && (12)\\ h'_2 &= h_2 - 0.5 r_{\mathrm{e}}\beta^2 && (13)\\ \theta_{\mathrm{e}} &= \arcsin\left(\frac{h'_1}{X_1}\right) = \frac{\pi}{2} - \theta_{\mathrm{i}} && (14) \end{aligned}$$

where θ_{i} and θ_{e} are defined as the incident angle and the elevation angle (for grazing angle, $\theta_{\mathrm{e}} \approx 0$), respectively. R and σ_{h} represent the specular reflection coefficient [15] and the standard deviation of the surface height distribution, respectively. Parameter h'_1 and h'_2 represent the corresponding effective antenna heights shown in Fig. 3. The effective reflection coefficient is smaller than the specular reflection coefficient and decreases with increasing wave height standard deviation.

2) Shadowing effect for the reflected ray: The sea surface may shadow other points on the surface (shown in Fig. 4(b)) especially when the elevation of the incident ray is small. Therefore, we take this shadowing effect into consideration by introducing a shadowing coefficient S_{fun} proposed by Smith [18] in our REL model, which can be expressed by:

$$S_{\mathrm{fun}} = \frac{1 - 0.5\mathrm{erfc}\left(\frac{\cot\theta_{\mathrm{i}}}{\sqrt{2}\beta_0}\right)}{\Lambda(\cot\theta_{\mathrm{i}}) + 1} \tag{15}$$

where

$$\Lambda(\cot\theta_{\mathrm{i}}) = \frac{1}{2}\left(\sqrt{\frac{2}{\pi}}\frac{\beta_0}{\cot\theta_{\mathrm{i}}}\exp^{-\frac{\cot\theta_{\mathrm{i}}^2}{2\beta_0^2}} - \mathrm{erfc}\left(\frac{\cot\theta_{\mathrm{i}}}{\sqrt{2}\beta_0}\right)\right) \tag{16}$$

where erfc and ${\beta_0}^2$ represent the complementary error function and the mean-square surface slope of the waves, respectively. The measured rms surface slope β_0 is usually within the range [0.04, 0.07] [17]. The shadowing effect is introduced by multiplying the shadowing coefficient S_{fun} with the effective coefficient R_{rough}. The shadowing coefficient is studied by using different rms surface slopes β_0 and the same antenna heights as our measurement campaign ($h_1 = 14.1\ \mathrm{m}, h_2 = 9.5\ \mathrm{m}$) in Fig. 5, from which it can be found that the reflected ray will be totally shadowed beyond the distance D_0 (24.4 km for $h_1 = 14.1\ \mathrm{m}, h_2 = 9.5\ \mathrm{m}$) where the LOS becomes a tangent to the surface of the earth. It also can be seen that larger β_0, corresponding to steeper slopes of the waves, results in smaller S_{fun} (more pronounced shadowing) at the same TX-RX distance.

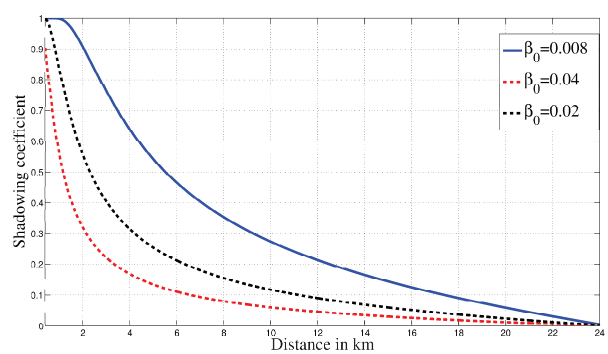

Fig. 5. Shadowing coefficient with different rms surface slope as a function of distance ($h_1 = 14.1\ \mathrm{m}, h_2 = 9.5\ \mathrm{m}$).

3) Divergence effect: Fig. 6 shows that the power density of the reflected ray can vary (beyond the usual ”thinning out” in free space) with TX-RX distances due to the earth curvature, which is defined as divergence effect. It can not be ignored in long-distance communications including maritime communications. In our REL model, the divergence effect is taken into consideration by multiplying the effective reflection coefficient

R_{rough} with a divergence coefficient Δ [19] expressed by:

$$\Delta = \begin{cases} \frac{1}{\sqrt{1+\frac{2D_1D_2}{r_{\mathrm{e}}(h_1'+h_2')}}} & \text{if } h_1'>0, h_2'>0 \\ 0 & \text{otherwise} \end{cases} \tag{17}$$

where h_1' and h_2' can be found in (12-13). D_1 and D_2 are also used in (4).

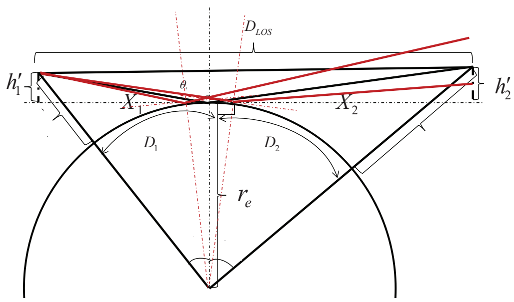

Fig. 6. Divergence effect in red.

Figure 7 shows the divergence coefficient Δ, obtained from (17) by setting $h_1 = 14.1$ m, $h_2 = 9.5$ m. We see that the divergence factor decreases with increasing TX-RX distance. Finally, the power of the reflected ray will decay to zero at the TX-RX distance of D_0, which is also consistent with the shadowing effect.

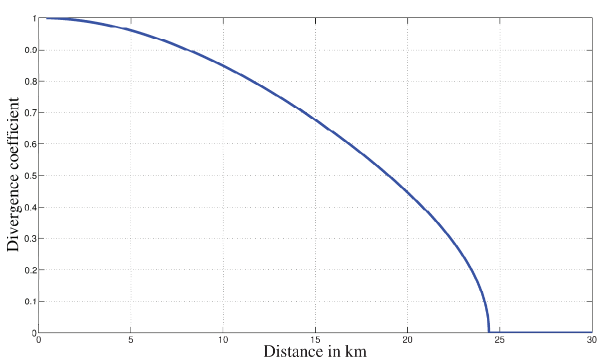

Fig. 7. Divergence factor as a function of distance.

4) Diffraction loss: Diffraction will make the radio transmission feasible even beyond the LOS though at the price of a diffraction loss. The diffraction theory of ground-wave propagation over a smooth spherical earth has been proposed in [20], [21], [22], which can be applied to the geometrical environments of the open sea. Referring to [22], the total distance d of the radio link is divided into three parts d_1, d_2, d_3, which is given by using (18) and shown in Fig. 8.

$$d = d_1 + d_2 + d_3 \tag{18}$$

where d_1 and d_2 are the distances to the horizon which can be calculated by using:

$$d_n = \sqrt{2k_{\mathrm{e}}r_{\mathrm{e}}h_{\mathrm{n}}} \qquad \text{n=1,2} \tag{19}$$

Here, h_1, h_2 represent the TX and RX antenna height, respectively as displayed in both Fig.3 and Fig.8. The effective earth radius is defined as the value for the radius of the earth that can be used in place of the actual radius to correct for refraction by the atmosphere. k_{e} is the ratio of the effective earth radius and true earth radius.

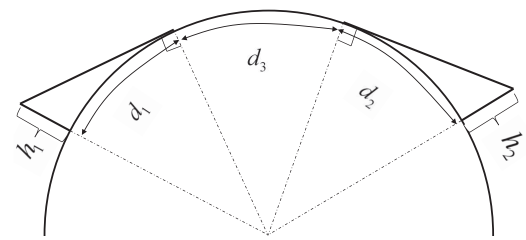

Fig. 8. Radio link beyond LOS over a smooth earth.

Each part will cause a corresponding loss $L_{\mathrm{n}}, n = 1, 2, 3$. The losses in dB L_1 and L_2 are always positive leading to a reduction of the RSL, which are obtained by using:

$$L_1 = 20\log_{10}\frac{N_1}{\sqrt{5.656\pi\zeta_1}} \tag{20}$$

$$L_2 = 20\log_{10} N_2 \tag{21}$$

where

$$20\log_{10} N_{\mathrm{n}} = -0.5 + 35\log_{10}\zeta_{\mathrm{n}} + 10\log_{10} F_{\mathrm{s}} \tag{22}$$

$$\zeta_{\mathrm{n}} = \frac{\frac{2\pi d_{\mathrm{n}}}{\lambda}}{\left(\frac{2\pi k_{\mathrm{e}} r_{\mathrm{e}}}{\lambda}\right)^{\frac{2}{3}}} \qquad \text{n=1,2,3} \tag{23}$$

and $10\log_{10} F_{\mathrm{s}}$ is approximated in this paper from Fig. 13 in [22] by using a polynomial function:

$$10\log_{10} F_{\mathrm{s}} = -0.024{\zeta_{\mathrm{n}}}^3 + 0.5438{\zeta_{\mathrm{n}}}^2 + 2.0391\zeta_{\mathrm{n}} - 0.4403 \tag{24}$$

L_3 is calculated by using the following polynomial function, which is obtained by curve fitting of Fig. 13 from [22]:

$$L_3 = 0.0086{\zeta_3}^3 + 0.2063{\zeta_3}^2 + 11.0997\zeta_3 - 0.8934 \tag{25}$$

The above approximations are valid when ζ_3 and ζ_{n} are less than 10. It also needs to be pointed out that d_3 can be 'mathematically' negative when the total TX-RX distance d is shorter than the sum of d_1 and d_2 (The direct path is beyond the horizon). In this case, the diffraction loss L_3 is negative and makes the total diffraction loss less than $L_1 + L_2$. It also may happen that the total diffraction loss L can be negative, when d is so short that $|L_3| > L_1 + L_2$. To avoid such situations, the total diffraction loss L is set to zero, if the $|L_3|$ is not less than $L_1 + L_2$. To summarize, the total diffraction loss L_{dif} in dB for both the direct path and the reflection path can be obtained by:

$$L_{dif} = \begin{cases} L_1 + L_2 + |L_3| & \text{if } d \geq d_1 + d_2 \\ L_1 + L_2 - |L_3| & \text{if } D_{06} < d < d_1 + d_2 \\ 0 & \text{if } d < D_{06} \end{cases} \tag{26}$$

The TX-RX distance for $L = L_1 + L_2 + L_3 = 0$ coincides with the path length D_{06} of a clearance of 0.6 in the First Fresnel Zone (FFZ) mentioned in the ITU recommendation [9] and obtained by using:

$$D_{06} = \frac{D_{\mathrm{f}} \cdot D_{\mathrm{h}}}{D_{\mathrm{f}} + D_{\mathrm{h}}} \quad km \tag{27}$$

$$\text{frequency-dependent term}: \quad D_{\mathrm{f}} = 38.9 f h_1 h_2 \tag{28}$$

$$\text{asymptotic term}: \quad D_{\mathrm{h}} = 4.1(\sqrt{h_1} + \sqrt{h_2}) \tag{29}$$

TABLE II
THE REL MODEL PARAMETER VALUES USED IN FIG. 10

Parameters	Values
RX antenna height for ant2	14.1 m
TX antenna height	9.5 m
β_0	0.008
σ_h	0.25
k_e	1

Here, f denotes frequency in GHz. The obtained total diffraction loss L with the same antenna heights as our measurement campaign ($h_1 = 14.1$ m$, h_2 = 9.5$ m) is shown in Fig 9, where $D_0 = d_1 + d_2 = 24.4$ km and $D_{06} = (7.8$ km, respectively.

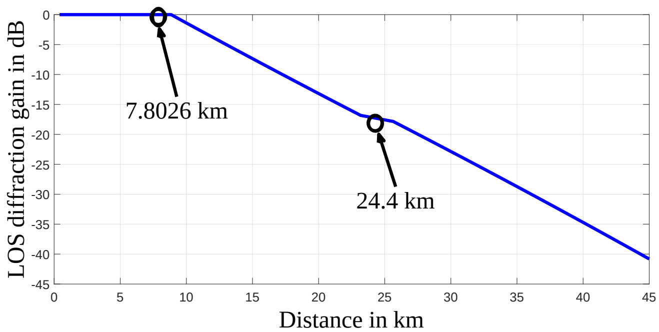

Fig. 9. LOS diffraction gain for $h_1 = 14.1$ m$, h_2 = 9.5$ m, as a function of distance.

C. Round Earth Loss Model

All the propagation effects listed in (1) have been investigated in detail in the above paragraphs. Even though the reflected ray will be completely eliminated by shadowing and divergence effects beyond a TX-RX distance of D_0 (Figs.5 and 7), the diffraction effect is considered to influence both the direct ray and the reflected ray. By integrating all these propagation effects into the geometrical model for the REL shown in Fig. 3, (2) has been improved to a REL model expressed by using:

$$P_{\mathrm{loss}} = 20\log_{10}\left(\frac{\lambda}{4\pi D_{\mathrm{LOS}}}\right) + 20\log_{10}(\eta) + L_{dif} \quad (30)$$

$$\eta = |1 + S_{\mathrm{fun}} \cdot \Delta \cdot R_{\mathrm{rough}} \cdot exp(jkD_{\mathrm{diff}})| \quad (31)$$

D. Comparison with measurements

Fig. 10 shows a comparison between the measured RSL and the three theoretical path-loss models including the PEL model, ITU model and our REL model (30-31). The measured values are averaged over a window to eliminate small-scale fading (see Sec. IV). The parameter values used for evaluations are listed in Table II, which are consistent with our measurement campaign setups. Since the weather conditions during the long-distance measurement campaign were rather stable and calm, the standard deviation of surface height distribution σ_h in (11) and the mean-square surface slope β_0 in (15) are set to small values (see table II) corresponding to small wave roughness. The Root Mean Square Error between the theoretical model and measurement data is widely used as a low-complexity comparison metric for model selection [23], [24]. Both the corresponding RMSE results in Table III and the comparison results in Fig.10 demonstrate that our REL model provides a good match to the measurement results. It also can be verified in Fig.10 that the ITU model does not take the fading dips (> 10 dB) at short TX-RX distances into consideration, while the PEL and REL models predict these well. On the other hand, the PEL model, which does not take the sea surface roughness, divergence and diffraction loss under different weather conditions into consideration, can not provide accurate predictions especially when TX-RX distances are beyond D_{06}, the 0.6 Fresnel clearance path length. In conclusion, our REL model matches the measurement results best with acceptable complexity and high adaptivity.

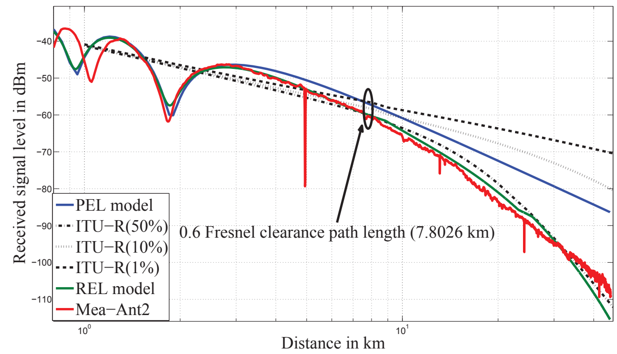

Fig. 10. Comparison between the REL model, the PEL model, ITU-R model and the long-distance measured RSL.

TABLE III
THE RESULTS FOR THE RMSE BETWEEN THE PATH-LOSS MODELS AND THE MEASURED RESULTS

Models	Values
PEL model	10.1
ITU-R (50%)	3.5
ITU-R (10%)	14.2
ITU-R (1%)	18.1
REL MODEL	1.9

E. Evaluation of the model parameters

The effects on RSL due to the variance of the sea surface roughness are worthwhile to be investigated, since the weather conditions over sea can change very quickly. It needs to be pointed out the antenna pattern mismatch due to boat movement is not taken into account in this evaluation. In this subsection, different sea surface parameters β_0 and σ_{h} (the rest of parameter values are the same as in Table I) are evaluated in the REL model and the corresponding results are displayed in Fig. 11 and Fig. 12, respectively. These effects of the reflected path vanish in Fig. 11 and Fig. 12 when $d \geq D_0$ since the reflected path will be eliminated by the shadowing and divergence effects discussed in the previous sections (see Fig. 5 and Fig. 7). It also can be found that the larger β_0 and σ_{h} parameters, corresponding to harsher weather conditions, result in decreased power of the reflected path. Hence, the deep fades at short TX-RX distances become shallower. To conclude, the RSL obtained from the REL model is independent of β_0 and $\sigma_{\rm h}$ when the TX-RX distance is beyond D_0 and the shadowing and scattering effect will only influence the amplitudes of the deep fades within the distance of D_0. From the above conclusion, together with the trends shown in Fig. 10 and Table III, the ITU-R (50%) model is also capable of predicting path loss with good accuracy in agitated seas.

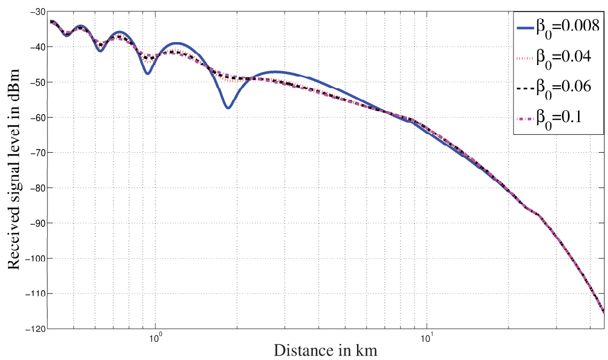

Fig. 11. REL with different mean-square surface slope β_0 (σ_h=0.25).

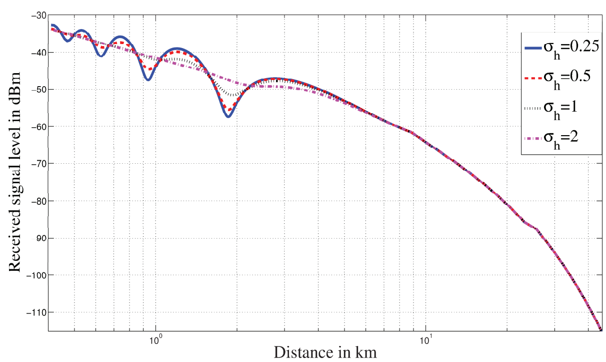

Fig. 12. REL with different standard deviation of surface height distribution σ_h (β_0=0.008).

IV. Small-Scale Channel Properties

The multi-path propagation can give rise to constructive and destructive superposition of the multipath components (MPCs) and thus lead to fluctuations of the received signal level, which is defined as small-scale fading [15]. The properties of the small-scale fading play an important role for nearly every aspect of receiver design: dynamic range, diversity, adaption of modulation scheme, and error-correction coding [25], [26]. The small-scale fading for maritime propagation environments at 1.9 GHz and 5.2 GHz has been investigated in [27] and [28], respectively. The propagation effects discussed in the previous sections can influence not only the path loss but also the small-scale channel properties, which can depend on location, frequency and sea conditions. Therefore, it will be meaningful to study the small-scale channel properties based on our measurement data. In [29], the previous analysis of the measurement data shows that the radio channel can be regarded as non frequency-selective over a bandwidth of 20 MHz. Therefore, the amplitude PDF of flat fading is studied in this section.

To determine the normalized envelope PDF, we first establish a set of functional forms that are commonly used for characterizing small-scale fading. The parameters for each of those functional forms are then determined by maximum-likelihood estimation, so that we obtain the parameterizations that best approximate the measured data. Finally, the best functional form is selected through application of the Akaike Information Criterion (AIC). This approach, first proposed in [30], was shown to have advantages compared to, e.g., Kolmogorov-Smirnov (KS) tests, and has been used successfully in a number of channel modeling papers since (e.g., [31]). In our study, the AIC is implemented to search the best-fit amplitude distribution of the measurement data among 7 common distributions: Lognormal distribution, Nakagami distribution, Normal distribution, Rician distribution, Two-Wave with Diffuse Power (TWDP) distribution [32], Rayleigh distribution and Weibull distribution. This selection is motivated by the fact that Weibull, Rayleigh, Rician and Normal distributions have been used to fit the measurement results in [28]. Lognormal distribution, which is commonly used to characterize shadowing by objects, is also used for fitting because the TX-RX radio link was blocked by several passing-by ferries at the distance of 5 km, which can be observed in Fig. 10. The scattering and two paths geometry make the TWDP distribution intuitively appealing for maritime environments. In our analysis, the large-scale channel properties have been removed by subtracting the averaged signal levels (averaging window: 10 wavelengths). Fig. 13 shows by color coding which distribution gives the best fit at what distance and the overall estimated distribution along the whole route. It needs to be pointed out that the boat was changing the direction at the distance between 100 m to 400 m, which makes the estimated best-fit distribution diverse. The corresponding percentages of the best-fit distributions are shown in the table IV.

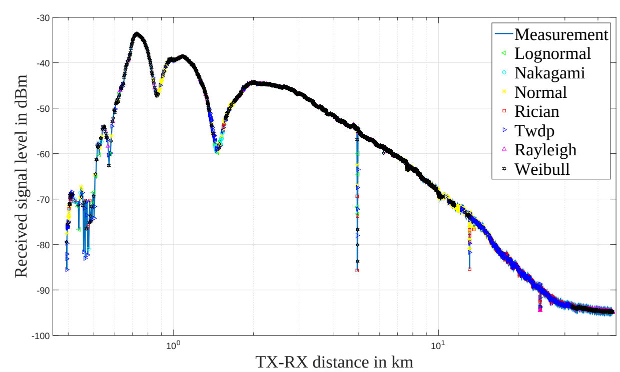

Fig. 13. Overall estimated best-fit distribution.

A. *Lognormal distribution*

The lognormal distribution is expressed as:

$$f(x|\mu,\sigma)=\frac{1}{x\sigma\sqrt{2\pi}}exp\{\frac{-(\ln x-\mu)}{2\sigma^2}\};x>0 \qquad (32)$$

where μ and σ represent the mean amplitude and standard deviation on a logarithmic scale, respectively. The boat turning at the initial distance and blocking of the radio link due to

TABLE IV
THE PERCENTAGE OF BEST-FIT DISTRIBUTION

Lognormal distribution	0.1241 %
Nakagami distribution	2.1096 %
Normal distribution	16.6081 %
Rician distribution	39.2606 %
TWDP distribution	4.4674 %
Rayleigh distribution	15.9721 %
Weibull distribution	21.4374 %

a passing-by ferry results in a shadowing effect, which is coincident with the occurrence of a Lognormal distribution in our path-loss measurements (see Fig. 10) [10]. Note that Fig. 14 only shows the parameters at those points for which the lognormal distribution is the best.

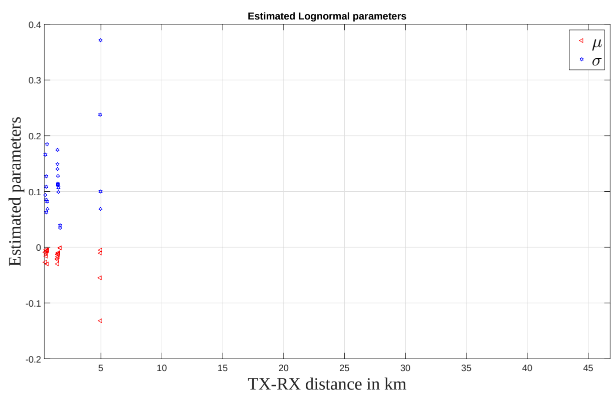

Fig. 14. Estimated parameters of Lognormal distribution.

B. Nakagami distribution

The Nakagami distribution is expressed by:

$$f(x|\mu,\omega) = 2(\frac{\mu}{\omega})^{\mu}\frac{1}{\Gamma(\mu)}x^{(}2\mu-1)exp\{\frac{-\mu}{\omega}x^2\};x>0 \quad (33)$$

where μ and ω represents the shape parameter and the scale parameter, respectively. The gamma function Γ can be expressed as:

$$\Gamma(\mu) = \int_0^{+\infty} t^{\mu-1}e^{-t}dt \quad (34)$$

The estimated parameters can be found in the Fig. 15.

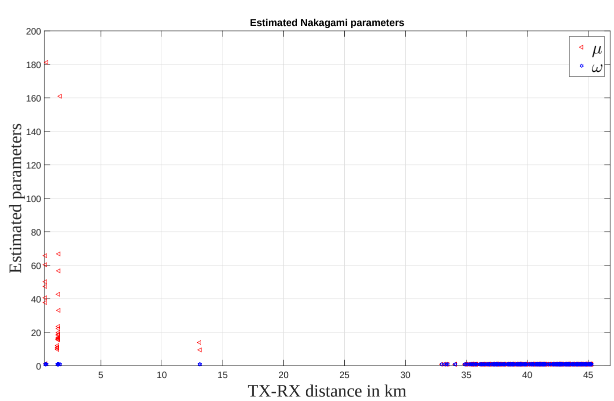

Fig. 15. Estimated parameters of Nakagami distribution.

C. Normal distribution

The Normal distribution is:

$$f(x|\mu,\sigma) = \frac{1}{\sigma\sqrt{2\pi}}exp\{\frac{-(x-\mu)^2}{2\sigma^2}\};x>0 \quad (35)$$

where μ and σ are mean and standard deviation, respectively. The estimated parameters can be found in Fig. 16. The Normal distribution is a good approximation for a Rician distribution with large k-factors. This is consistent with a strong LOS and a highly correlated reflected path and a weaker diffuse component.

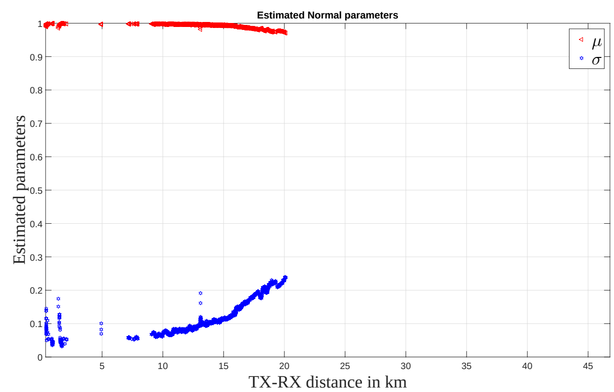

Fig. 16. Estimated parameters of Normal distribution.

D. Rician distribution

The Rician distribution is expressed by using:

$$f(x|s_1,\sigma) = \frac{x}{\sigma^2}exp\{\frac{-(x^2+s_1^2)}{2\sigma^2}\}I_0(\frac{xs_1}{\sigma^2});x>0 \quad (36)$$

where s_1 and σ represent the non-centrality parameter and the scale parameter, respectively. $I_0(\cdot)$ is the 0th-order modified Bessel function of the first kind [33]. The estimated parameters can be found in Fig. 17, from which it can be seen that the Rician distribution occurs at the distances between 15 km and 45 km. It can also be clearly seen that the Rice K-factor ($\frac{s_1{}^2}{\sigma^2}$) decreases with distance, which agrees with the intuition that the diffuse part increases and the direct path decreases in the signal strength with distance.

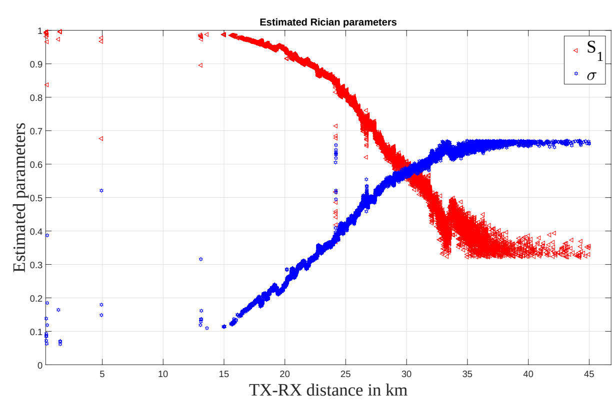

Fig. 17. Estimated parameters of Rician distribution.

E. TWDP distribution

The TWDP distribution is expressed as:

$$
\begin{aligned}
f(x|s_1, s_2, \sigma) = \frac{x}{\sigma^2} exp\{\frac{-(x^2 + {s_1}^2 + {s_2}^2)}{2\sigma^2}\} \cdot \\
\frac{1}{\pi} \int_0^{\pi} exp(\frac{s_1 s_2 cos\theta}{\sigma^2}) \cdot \\
I_0(\frac{x}{\sigma^2} \sqrt{{s_1}^2 + {s_2}^2 - 2 s_1 s_2 cos\theta}) d\theta; x > 0
\end{aligned}
\tag{37}
$$

where s_1 and s_2 represents the amplitude of the direct and reflected path, respectively. σ is the scale parameter and can be interpreted as the standard deviation of the diffuse contribution. The estimated parameters are shown in Fig. 18, from which it can be found that the TWDP distribution mostly occurs at the distances between 9 km and 35 km. Overall the TWDP distribution and Rician distribution dominate the distance between 9 km and 45 km. The TWDP distribution and Rician distribution are related to each other, depending on the correlation between the direct path and the reflection path. If the correlation is high, the direct path and the reflection path can be regarded as the same path and the amplitude distribution of the received signal follows a Rician distribution. This can be seen from the estimated results between 35 km and 45 km, where the distance is beyond D_0 (24.4 km) and the reflected path and the direct path are highly correlated due to the earth curvature. Since the AIC penalizes the use of distributions with more adjustable parameters, in this case a Rice distribution will be selected. Similarly, if the correlation is low, the direct path and the reflection path can be easily distinguished. In this case, the amplitude distribution of the received signal turns out to be a TWDP distribution. This can be shown by the estimation results between 9 km and 15 km, where the distance is within D_0 (24.4 km). The correlation between the paths is influenced by the boat movement, wave surface and TX-RX distance. It is also mentioned in [32] that the difference between TWDP distribution and Rician distribution is small when the Rice K factor is less than 3 dB, which is consistent with our measurement results.

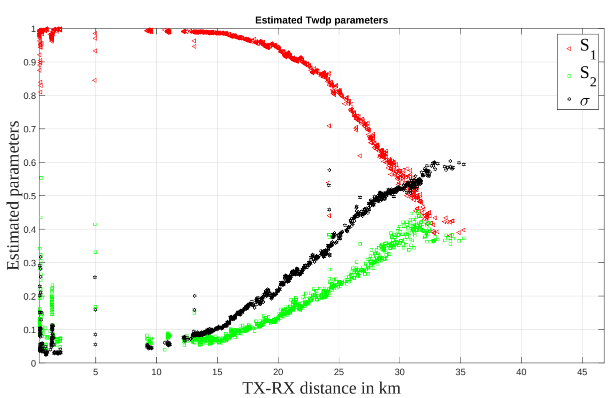

Fig. 18. Estimated parameters of TWDP distribution.

F. Rayleigh distribution

The Rayleigh distribution is expressed as:

$$f(x|\sigma) = \frac{x}{\sigma^2} exp\{\frac{-x^2}{2\sigma^2}\}; x > 0 \tag{38}$$

where σ is the standard deviation of the underlying Gaussian distribution. The estimated parameters can be found in Fig. 19, from which it can be seen that the Rayleigh distribution occurs at the distances between 35 km and 45 km. The direct path is beyond the horizon and the amplitude distribution of the received signal is changed from a Rician distribution to a Rayleigh distribution. The latter is a special case of the former, with s=0. As it has fewer parameters, AIC will select it when the Rice factor is small.

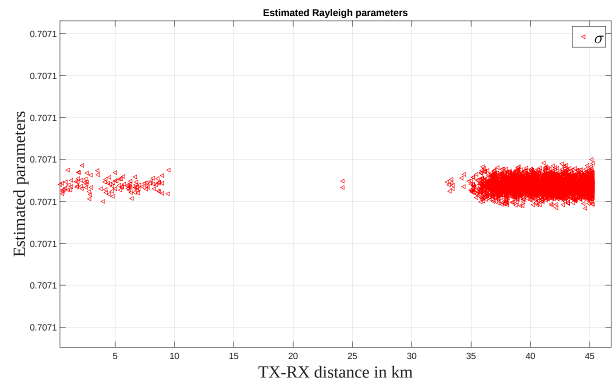

Fig. 19. Estimated parameters of Rayleigh distribution.

G. Weibull distribution

The Weibull distribution is expressed by using:

$$f(x|a, b) = \frac{b}{a}(\frac{x}{a})^{b-1} exp\{-(\frac{x}{a})^b\}; x > 0 \tag{39}$$

where a and b represent the scale parameter and the shape parameter, respectively. The estimated parameters can be found in Fig. 20, from which it can be seen that the Weibull distribution occurs at the beginning and the end of the route.

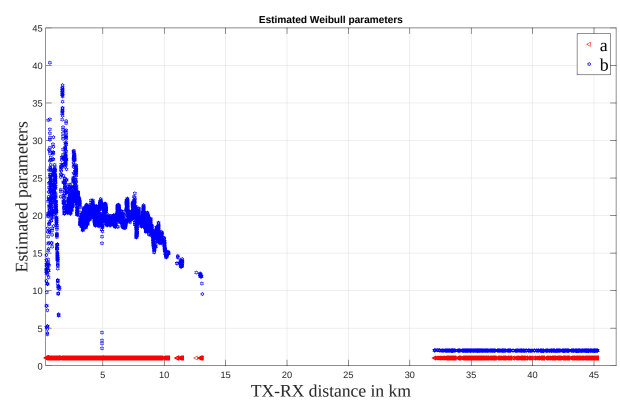

Fig. 20. Estimated parameters of Weibull distribution.

H. Fading distribution function

Table V lists the distributions that are found to be the best-fit in the various specific region.

The TWDP distribution is considered to be very interesting for the maritime propagation environment, since the propagation scenario there fits well with the fundamental assumptions

TABLE V
DOMINANT DISTRIBUTION IN DIFFERENT REGIONS

dominant distribution	range in km	incident rate
Weibull	[0.39, 9.2]	88%
Normal	[9.2, 15.6]	82.2%
Rician	[15.6, 35.7]	82.1%
Rayleigh	[35.7, 45.3]	67.7%

about TWDP due to the suitable environmental geometry. According to our measurements, it indeed provides the best fit for short distances. However, the TWDP does not turn out to be the best fit for any of the larger regions. Fig. 21 shows the percentage of incident rate at certain TX-RX distances where TWDP is the best fit distribution. It can be found that in the distance range of [0.4, 2.1] km and [9.2, 35.2] km there is an appreciable percentage of points where the TWDP distribution is the best fit. Furthermore, TWDP can be used as the overall best-fit distribution. When the reflection is reduced, TWDP asymptotically becomes Rice (as a special case) where a LoS component is present and then when due to earth curvature LoS is lost, Rice degrades to Rayleigh.

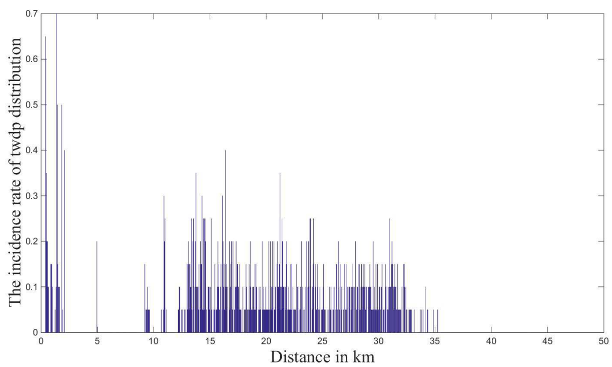

Fig. 21. The incident rate of TWDP distribution.

I. Spatial correlation

Multi-antenna techniques can be used to obtain spatial diversity whose effectiveness depends on the correlation of the signals at the different antenna elements. The correlation between the two RX antenna's outbound RSL in our experimental setup (shown also in [10]) is characterized by the correlation coefficient [15]:

$$P_{xy} = \frac{E\{x.y\} - E\{x\}E\{y\}}{\sqrt{(E\{x^2\} - [E\{x\}]^2)(E\{y^2\} - [E\{y\}]^2)}} \tag{40}$$

where x and y represent the amplitude of the receive signal from the two RX antennas, respectively. A 128 sec averaging "window" is used to calculate the expectation. The result in Fig. 22 shows that the correlation coefficient is above 0.7 when the distance is in the range of [2.92, 3.55] km, showing that the two channels are highly correlated. On the other hand the correlation coefficient decreases with increasing TX-RX distance. It needs to be pointed out that the channel turns out to be independent (correlation coefficient is close to 0), when the TX is below the horizon (TX-RX distance is over $D_0 = 24.4$km). This indicates the potential benefits of employing multi-antenna techniques for maritime communication systems with a similar antenna setup. In addition, the two RX channels are essentially uncorrelated at the distance of 4.8 km and 13.5 km, which is caused by the shadowing effect of the passing-by ships. Therefore, the shadowing effect caused by passing-by ships can reduce the spatial correlation between the two RX channels.

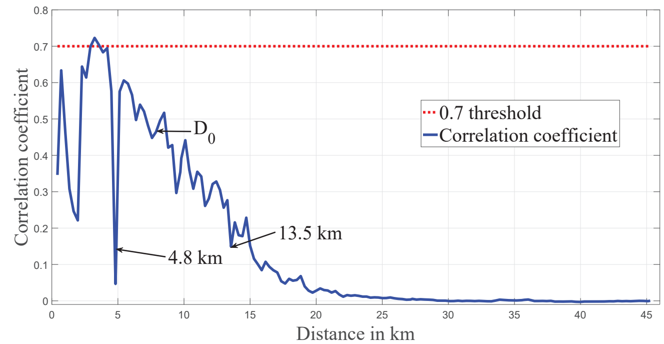

Fig. 22. Correlation coefficient derived from the outbound trip measurements.

V. CONCLUSIONS

A new path-loss model for the open-sea environment is presented based on a geometrical model of the round earth. With increasing TX-RX distance, the LOS ray will experience diffraction effects, while the reflected ray will be influenced by the scattering, shadowing, divergence and diffraction effects. We describe, motivate, and model all of these effects, and find a complete model incorporating all of these aspects. The REL model has been validated by long-distance measurement results, and it fits the measurement very well according to the RMSE results. Different channel parameters related to the sea surface roughness were analyzed, and it is found that the effects due to sea roughness vanish when the TX-RX distance is beyond D_0.The amplitude distribution of the received signal turns out to be Weibull at short TX-RX distances between 0.4 km and 9 km. The TWDP distribution, Rician distribution and Rayleigh distribution dominate at distances between 9 km and 45 km. The parameters of the small-scale fading are modeled as a function of distance. Finally, the signals at two vertically separated (by 3 m) antennas turn out to be de-correlated at large TX-RX distance, especially when the TX is below the horizon, which suggests to employ multi-antenna techniques for maritime communication systems with a similar antenna setup. Even though the REL model is valid for distances up to 45 km in the Norwegian cold sea with calm weather conditions, further validation is needed for scenarios with different sea conditions and longer ranges.

ACKNOWLEDGEMENT

The authors would like to thank the Ming Hsieh Department of Electrical and Computer Engineering, University of Southern California, for hosting K. Yang for a research visit during which part of this work was done, and also thank P. H. Lehne at Telenor GBDR for his support with the channel sounder equipment that Telenor so kindly lent us. Furthermore, the practical support by T. Mathiesen from NTNU and K. Husby, O. Trandem and T. Gjelsvik from Sintef ICT, is highly appreciated for the practical part of the measurements that has been successfully performed. The measurements has been funded by the Norwegian Research Council through the MARCOM project coordinated by F. Bekkadal and K. Fjørtoft at Sintef Marintek, Trondheim, Norway.

References

[1] https://www.nkom.no
[2] Y. M. L. Roux, J. F. Mnard, C. Toquin, J. P. Jolivet, F. A. Nicols "Experimental measurements of propagation characteristics for maritime radio links," *proc. 9th International Conference on Intelligent Transport Systems Telecommunications, 2009. ITST09*, Oct, 2009.
[3] M. J. Lopes, F. Teixeira, J. B. Mamede, R. Campos, "Wi-Fi broadband maritime communications using 5.8 GHz band," *Underwater Communications and Networking (UComms)*, pp. 1C5, 2014.
[4] S. R. Saunders and A. Aragon-zavala, *Antennas and Propagation for Wireless Communication Systems*. . John Wiley & Sons, 2007.
[5] N. H. Lu, "Linearized, Unified Two-Ray Formulation for Prapagation over a Plane Earth," *proc. Sensor for Industry Conference, 2005. SIcon05*, Feb, 2005.
[6] J. Joe, S. K. Hazra, S. H. Toh, W. M. Tan, J. Shankar "Path Loss Measurements in Sea Port for WiMAX," *proc. IEEE Conference on Wireless Communications and Networking Conference, IEEE WCNC 2007*, 2007.
[7] Y. Lee, F. Dong, Y. Meng. "Near sea-surface mobile radiowave propagation at 5 GHz: measurement and modeling," *Radioengineering*, 23(3), pp. 824C830, 2014.
[8] K. Yang, T. Ekman, T. Røste, and F. Bekkadal "A quasi-deterministic path loss propagation model for the open sea environment," in *The 14th International Symposium on Wireless Personal Multimedia Communications, 2011. WPMC11*. Brest, France, Oct. 2011.
[9] ITU-R Recommendation P.1546-5, "Method for point-to-area predictions for terrestrial services in the frequency range 30 MHz to 3000 MHz," Sep. 2013.
[10] K. Yang, T. Røste, F. Bekkadal, K. Husby and O. Trandem "Long-distance propagation measurements of mobile radio propagation for the open sea at 2 GHz," *IEEE VTC Spring*, San Francisco, US, Sep. 2011.
[11] K. Yang, T. Røste, F. Bekkadal and T. Ekman, "Land-to-ship radio channel measurements over sea at 2 GHz," in *IEEE International Conference on Wireless Communications, Networking and Mobile Computing, 2010. WICOM2010*. Chengdu, China, Sep. 2010.
[12] K. B Kim, A. Maifuz, J. H. Lee, S. O. Park "Experimental Study of Propagation Characteristic for Maritime Wireless Communication," in *International Symposium on Antennas and Propagation (ISAP2012)*. Nagoya, Japan, Nov. 2012.
[13] W. Wang, G. Hoerack, T. Jost, R. Raulefs, M. Walter, U. C. Fiebig, "Propagation channel at 5.2 GHz in baltic sea with focus on scattering phenomena," in *9th European Conference on Antennas and Propagation (EuCAP)*. Paris, France, May. 2015.
[14] K. Yang, A. F. Molisch, T. Ekman and T. Røste "A Deterministic Round Earth Loss Model for Open-Sea Radio Propagation," *IEEE VTC Spring*, 2013 IEEE 77th, Dresden, 2013, pp. 1-5. doi: 10.1109/VTC-Spring.2013.6691821.
[15] A. F. Molisch, *Wirless Communications 2nd edition*. IEEE Press - Wiley, 2011.
[16] K. Kahma, D. Hauser, H. E. Krogstad, S. Lehner, J. A. J. Monbaliu, L. R. Wyatt "Measuring and Analysing the Directional Spectra of Ocean Waves," *EU COST Action 714, EUR 21367*, 465 p., ISBN 92-898-0003-8. 2005.
[17] Y. Karasawa and T. Shiokawa "Characteristics of L-Band Multipath Fading due to Sea Surface Reflection," *IEEE Transaction on antenna and propagation*, VOL. AP-32, NO. 6, June 1984.
[18] B. J. Smith, "Geometrical Shadowing of a Random Rough Surface," *IEEE Transaction on antenna and propagation*, VOL. AP-15, NO. 5, Sep 1967.
[19] J. D. Parsons, *The Mobile Radio Propagation Channel*. John Wiley & Sons, 2000.
[20] ITU-R Recommendation P.526-13 (2013), "Propagation by diffraction," Aug. 2014.
[21] K. A. Norton "The calculation of ground-wave field intensities over a finitely-conducting spherical earth," *Proc. IRE, Dec. 1941.*
[22] K. Bullington "Radio propagation above 30 megacycles," *Proc. IRE, Oct. 1947*.
[23] M. Farhoud, A. El-Keyi, A. Sultan, "Empirical correction of the Okumura-Hata model for the 900 MHz band in Egypt," Third International Conference on Communications and Information Technology (ICCIT), pp 386-390, 2013.
[24] I. Rodriguez, H. C. Nguyen, et al , et al."A Geometrical-Based Vertical Gain Correction for Signal Strength Prediction of Downtilted Base Station Antennas in Urban Areas," In Vehicular Technology Conference (VTC Fall), pp 1-5, 2012.
[25] E. Biglieri, J. Proakis and S. Shamai, "Fading channels: information-theoretic and communications aspects," IEEE Transactions on Information Theory, vol.44, no.6, pp.2619-2692, Oct 1998,
[26] M. K. Simon and Mohamed-Slim Alouini, "Digital communication over fading channels," Vol. 95. John Wiley & Sons, 2005.
[27] K. N. Maliatsos, P. Loulis, M. Chronopoulos, P. Constantinou, P. Dallas and , M. Ikonomou , "Measurements and Wideband Channel Characterization for Over-the-sea Propagation," in *IEEE International Conference on Wireless and Mobile Computing, Networking and Communications, 2006. WiMob 2006*. Montreal, Canada, Jun. 2006.
[28] W. Wang, R. Raulefs. and T. Jost,"Fading Characteristics of Maritime Propagation Channel for Beyond Geometrical Horizon Communications in C-Band," CEAS Space Journal. 10.1007/s12567-017-0185-1, 2017,
[29] K. Yang, T. Røste, F. Bekkadal, and T. Ekman "Experimental multipath delay profile of mobile radio channels over sea at 2 GHz," *IEEE LAPC*, loughborough, UK, Nov. 2012.
[30] U. G. Schuster and H. Bolcskei, "Ultrawideband Channel Modeling on the Basis of Information-Theoretic Criteria.", *IEEE Trans. on WIRELESS COMMUNICATIONS.* vol. 6, no. 7, pp. 2464–2475, July. 2007.
[31] C. C. Chong and S. K. Yong, "A Generic Statistical-Based UWB Channel Model for High-Rise Apartments.", *IEEE Trans. on Antenna and Propagation.* vol. 53, no. 8, pp. 2389–2399, Aug. 2005.
[32] G. D. Durgin, T. S. Rappaport and D. A. de Wolf, "New Analytical Models and Probability Density Functions for Fading in Wireless Communications.", *IEEE Trans. on WIRELESS COMMUNICATIONS.* vol. 50, no. 6, pp. 1005–1015, June. 2002.
[33] M. Abramowitz and I. A. Stegun, "Handbook of Mathematical Functions with Formulas, Graphs, and Mathematical Tables. Applied Mathematics Series 55 (10 ed.)," New York, USA: United States Department of Commerce, National Bureau of Standards; Dover Publications. ISBN 978-0-486-61272-0. LCCN 64-60036. MR 0167642.
[34] https://www.mathworks.com/help/matlab/ref/polyfit.html

Kun Yang received his M.Sc from University of Agder, Grimstad, Norway in 2007 and his Ph.D from Norwegian University of Science and Technology (NTNU), Trondheim, Norway in 2013. He was visiting the Wireless Devices and systems Group, University of Southern California in 2011 and Communications Theory Group, Eurecom, France in 2012, respectively. Since 2014, he founded a Norwegian startup, Super Radio AS, which is maritime 5G test solution provider for small-version yara-birkeland autonomous boat and high-resolution channel sounding solution provider. From 2015 to 2016, He was with IFSTTAR as PostDoc and worked on mmw channel sounding for regional train in a EU Rail2shift lighthouse project.

His current research interests include radio channel measurement and modelling, Maritime broadband technology, massive MIMO technology and millimeter wave technology. He has received IEEE WCSP Best paper award in 2010. Since 2016, he is leading the world´s first maritime 5G project, MAMIME, funded by Norwegian Research council and participating several Norwegian national projects.

Andreas F. Molisch (S´89–M´95–SM´00–F´05) received the Dipl. Ing., Ph.D., and habilitation degrees from the Technical University of Vienna, Vienna, Austria, in 1990, 1994, and 1999, respectively. He subsequently was with FTW Research Center for Telecommunications (Austria), AT&T (Bell) Laboratories Research (USA); Lund University, Lund, Sweden, and Mitsubishi Electric Research Labs (USA). He is now a Professor and the Solomon Golomb – Andrew and Erna Viterbi Chair at the University of Southern California, Los Angeles, CA, USA.

His current research interests are the measurement and modeling of mobile radio channels, multi-antenna systems, wireless video distribution, ultra-wideband communications and localization, and novel modulation formats. He has authored, coauthored, or edited four books (among them the textbook Wireless Communications, Wiley-IEEE Press), 19 book chapters, more than 240 journal papers, more than 320 conference papers, as well as more than 80 patents and 70 standards contributions.

Dr. Molisch has been an Editor of a number of journals and special issues, General Chair, Technical Program Committee Chair, or Symposium Chair of multiple international conferences, as well as Chairman of various international standardization groups. He is a Fellow of the National Academy of Inventors, Fellow of the AAAS, Fellow of the IET, an IEEE Distinguished Lecturer, and a Member of the Austrian Academy of Sciences. He has received numerous awards, among them the Donald Fink Prize of the IEEE, the IET Achievement Medal, the Armstrong Achievement Award of the IEEE Communications Society, and the Eric Sumner Award of the IEEE.

Torbjörn Ekman was born in Vöterå, Sweden, in 1969. He received the M.Sc. degree in engineering physics in 1994 and the Ph.D. degree in signal processing in 2002, both from Uppsala University, Sweden. In 2006 he joined the Department of Electronics and Telecommunications at the Norwegian University of Science and Technology (NTNU) in Trondheim, Norway, where he now is a Professor. From 1997 to 1998 he was a visiting scientist at the Institute of Communications and Radio-Frequency Engineering, Vienna University of Technology, Vienna, Austria, on a Marie Curie Grant. From 1999 to 2002, he was visiting the Digital Signal Processing Group, University of Oslo, Norway. In 2002-2005, he made his postdoctoral studies at UniK, University Graduate Center, Kjeller, Norway.

His current research interests include signal processing in wireless communications, scheduling of radio resources, and dynamic modeling, and prediction of radio channels. He is currently participating in projects on costal and arctic maritime operations and surveillance, radio resource management and channel modeling.

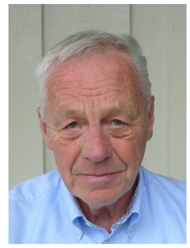

Terje Røste was born 1941, received his M.Sc from the The Norwegian Institute of Technology (NTH) in 1965, and his Ph.D at the same institute in 1970. In the years 1972-81 he was a senior scientist at SINTEF Electronics Research Laboratories (ELAB) in Trondheim, Norway. He was senior scientist and R&D manager at ABB Corporate Research, Norway (1983-1995) and later director of research in the telecommunication company Nera (1995-2000). He became an adjunct professor at the University of Oslo (1991-1998) in radio communications, and later an adjunct professor at the Norwegian University of Science and Technology (NTNU) (1998-2013). From 2001-2008 he was a senior R&D engineer in Nera Research participating in the development of mobile satellite communication systems. From September 2008 to March 2013 senior development engineer at Jotron Satcom AS developing stabilized antennas for VSAT between ship and land.

His main research interest as an adjunct professor was within adaptive pre-distortion techniques and adaptive dynamic biasing techniques for power amplifier efficiency enhancement, statistical channel modeling for broadband mobile radio access and channel modeling for radio propagation land to ship. He is a life member of IEEE and has been a reviewer of IEEE journal and conference papers. He is presently professor emeritus at NTNU and Consultant in Radio Engineering.

Marion Berbineau received the Engineer degree from Polytech'Lille (France) and the Ph.D. degree from the Univ. of Lille, both in electrical engineering, respectively in 1986 and 1989. She is a full time Research Director at IFSTTAR that is equivalent to Professor. She is expert in the fields of radio wave propagation in transport environments (tunnels), electromagnetic modeling, channel characterization and modeling, MIMO, wireless systems for telecommunications, cognitive radio for railways and GNSS localization-based for ITS particularly for the rail and public transport domains. She is active as an expert for the GSM-R and future systems like LTE-A or 5G. She is involved in several National and European research projects. She is author and co-author of several publications and patents.